Supplement of Ocean Sci., 22, 1409–1427, 2026
https://doi.org/10.5194/os-22-1409-2026-supplement
© Author(s) 2026. CC BY 4.0 License.

Ocean Science Open Access EGU

Supplement of

Sea-surface temperature variability and climate drivers in Cuba's Jardines de la Reina National Park (2003–2022)

Maibelin Castillo-Alvarez et al.

Correspondence to: Maibelin Castillo-Alvarez (mcastilloa@udec.cl) and Oscar Pizarro (opizarro@udec.cl)

The copyright of individual parts of the supplement might differ from the article licence.

S1. SST data validation.

A comparison between MUR SST (used as the primary high-resolution product), ERA5 SST, and GLORYS12 mixed-layer temperature over the full study domain and period is summarized using a Taylor diagram (Figure S1). Relative to the MUR reference point (normalized standard deviation = 1, correlation = 1), GLORYS12 falls markedly closer to the target, indicating higher pattern agreement and a smaller centered misfit ($r \approx 0.94$; normalized $\sigma \approx 1.27$; centered RMSD ≈ 0.46). In contrast, ERA5 exhibits weaker agreement with MUR and substantially larger variability amplitude ($r \approx 0.83$; normalized $\sigma \approx 1.67$; centered RMSD ≈ 1.00), consistent with a larger departure from the reference.

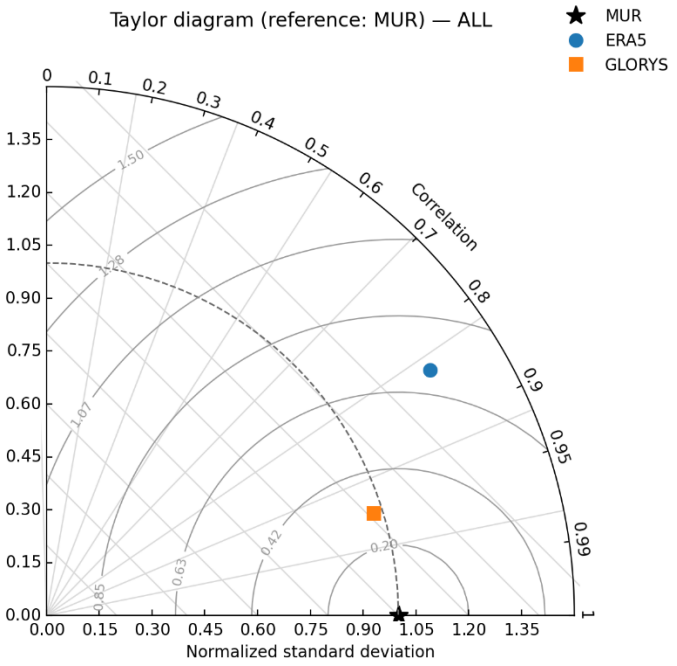

Figure S1. Taylor diagram comparing sea surface temperature (SST) from ERA5 and GLORYS12 against the MUR satellite product (reference). The diagram shows the normalized standard deviation, correlation coefficient, and centered root mean square difference (RMSD) for each dataset. This comparison highlights the relative performance and consistency of the reanalysis products with respect to satellite observations.

In addition, although continuous long-term in situ observations are not available for the region, we included an independent short-term comparison between MUR SST and temperature time series from two in situ sensors deployed within the Jardines de la Reina National Park during 2016 (February–June). These sensors were StowAway XTI models from the ONSET Company, which have a resolution of 0.01°C. More information about this data can be found in Gonzáles de Zayas et al. (2022). MUR SST reproduces the observed temporal variability well, with correlations ranging from $r \approx 0.8$–0.85, RMSE of ~0.8 -1.1 °C, and a modest cold bias consistent with known satellite skin–bulk differences (Figure S2).

These in situ comparisons are not intended as full validation, but rather as an independent consistency check that supports the use of MUR SST for describing spatial and temporal variability. Importantly, the core results of the study (seasonal phasing, relative shelf–offshore contrasts, interannual modes, and long-term trends) are robust across products and do not rely on absolute SST values at individual grid points.

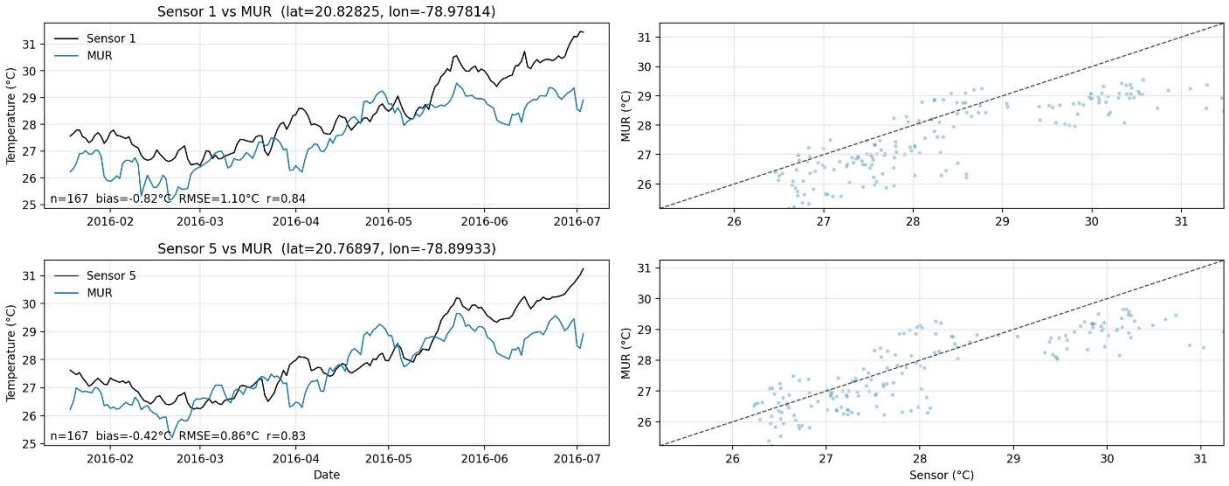

Figure S2. Comparison between in situ SST measurements from coastal sensors (Sensor 1 and Sensor 5) and satellite-derived SST from the MUR product at the corresponding locations. Left panels show the time series of temperature, while right panels display the scatter plots. Statistical metrics including sample size (n), bias, root mean square error (RMSE), and correlation coefficient (r) are indicated in each panel.

S2. Sensitivity of Box Selection.

To evaluate the robustness of our results to the exact definition of the GAM and CS subregions, we performed a box-selection sensitivity analysis in which SST anomalies were recomputed using multiple alternative boxes that vary in both location and spatial extent (Figure S5). Within GAM, the reference box (Square 1; ~25×25 km², blue) was compared against alternative boxes displaced within the gulf and with different sizes, including Squares 2, 3, and 8 (25×25 km², blue) and a smaller configuration (Square 11; ~13×13 km², red). Offshore in the CS, the reference box (Square 4; ~25×25 km², blue) was similarly compared against alternative offshore boxes spanning different positions and sizes (Squares 5–7 and 6; ~25×25 km², blue; Square 9; ~50×50 km², black; Square 10; ~100×100 km², magenta; and Square 12; ~13 ×13 km², red). The SST anomaly time series obtained from these alternative configurations remains highly consistent with those derived from the reference boxes: correlations with the GAM reference series range from r = 0.989 to 0.999, while correlations with the CS reference series range from r = 0.899 to 0.999 (Table S1). All correlations are statistically significant at ≥95% confidence. Overall, this analysis indicates that the temporal variability characterized in our study, and

thus the inferred gulf–offshore contrasts, is not sensitive to moderate changes in the position or size of the selected subregions.

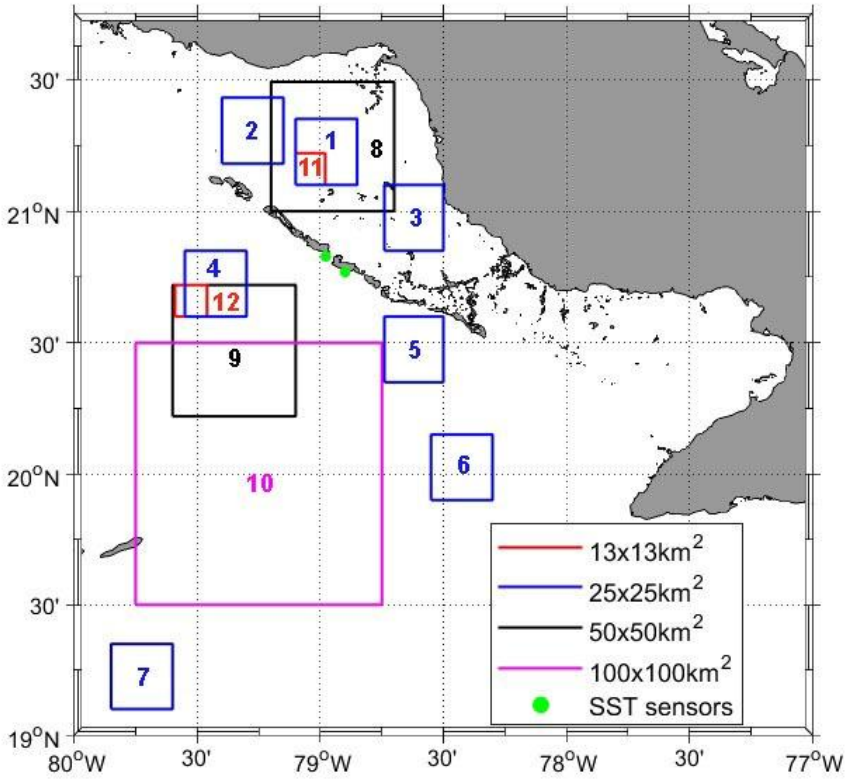

Figure S3. Alternative box configurations used to test the sensitivity of SST-anomaly time series to the definition of the Gulf of Ana María (GAM) and Caribbean Sea (CS) subregions. The reference regions are Square 1 (GAM; ~25×25 km²) and Square 4 (CS; ~25×25 km²). Alternative boxes were defined by shifting the box position and changing its spatial extent within GAM (Squares 2, 3, 8, and 11) and within the offshore CS region (Squares 5, 6, 7, 9, 10, and 12). Colors indicate box area: ~13×13 km² (red), ~25×25 km² (blue), ~50×50 km² (black), and ~100×100 km² (magenta). Green dots indicate the locations of in situ SST sensors used for an independent consistency check.

Table S1. Pearson correlations between SST-anomaly time series computed from the reference GAM and CS boxes (Squares 1 and 4, respectively) and from alternative box configurations shown in Figure S4. All correlations are statistically significant at ≥95% confidence.

Box N°1 (GAM) versus Box N°	*Correlation (r)*	*Box N°4 (CS) Versus Box N°*	*Correlation (r)*
2	0.996	5	0.960

3	0.989	6	0.930
8	0.999	7	0.899
11	0.999	9	0.999
		10	0.964
		12	0.996

S3. Comparison between EOF results based on monthly anomalies time series with and without linear trend removed.

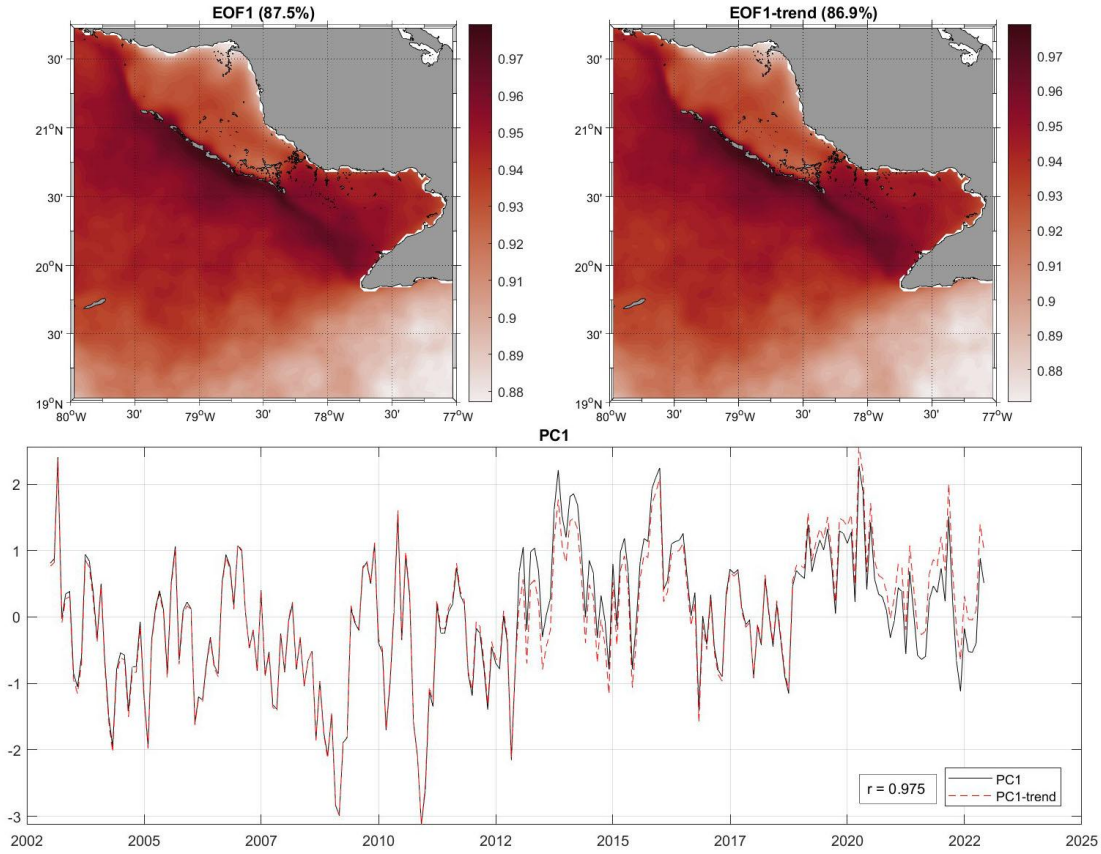

Figure S4a. EOF analysis of monthly SST anomalies for 2003–2022. Left up: spatial patterns of EOF1 (87.5 %), the input field consists of monthly anomalies with the linear trend removed. Right up: like the left panel but linear trends were not removed (in this case EOF 1 explains 86.9 % of the total variance). Down: Corresponding principal components PC1 with (PC1-trend) and without trend (PC1). The correlation coefficient between both time series is r=0.975 at zero lag.

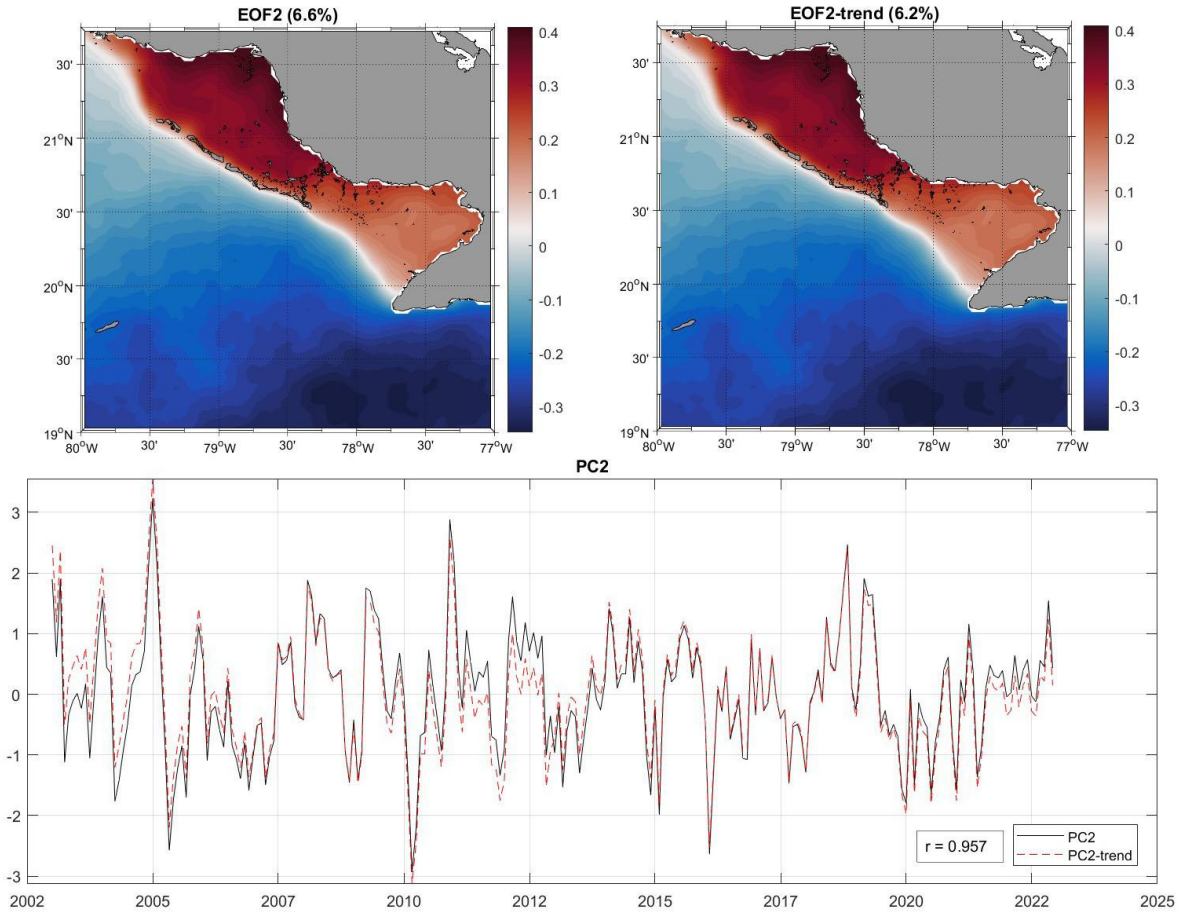

Figure S4b. Like Figure S3a, but for the second mode.

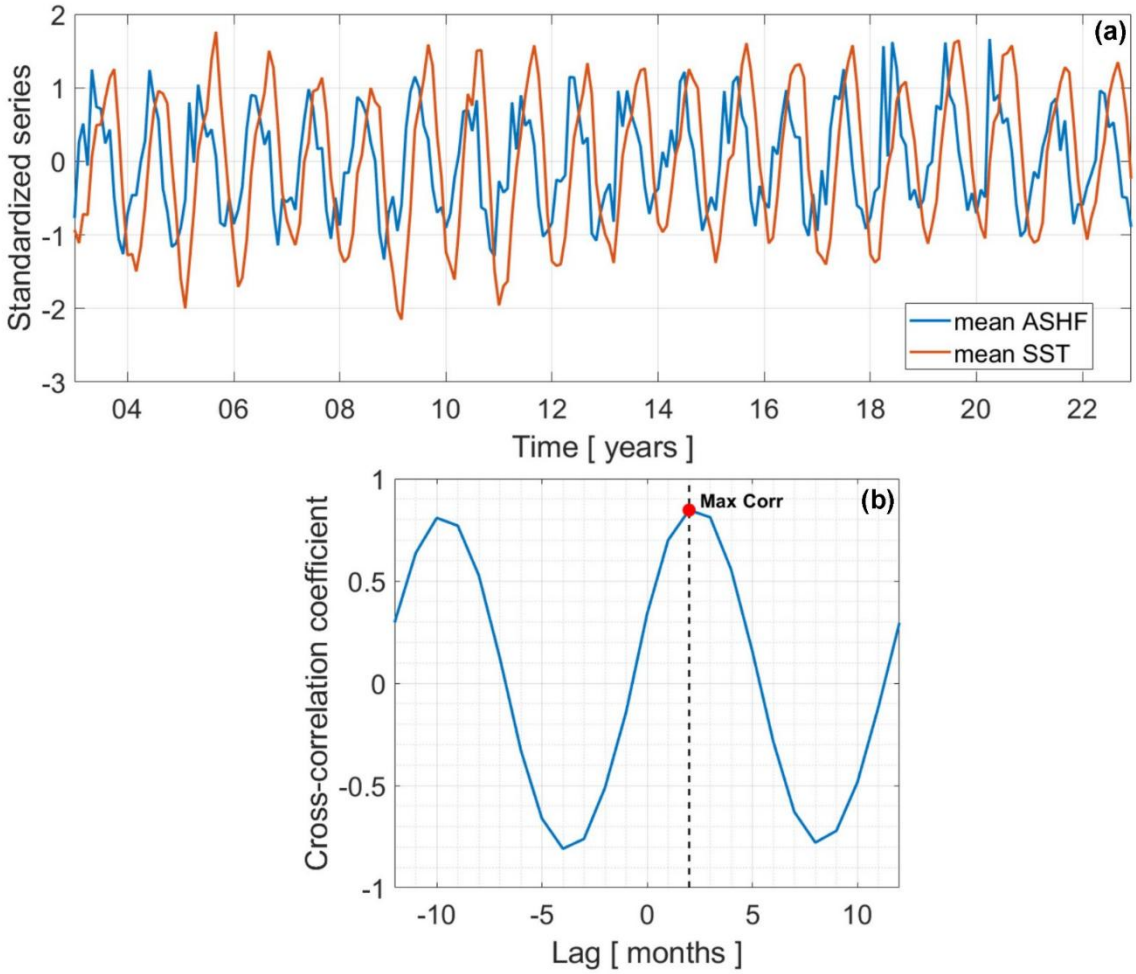

Figure S5. Standardized regional-mean monthly SST (orange) and air–sea heat flux (blue) time series over 2003–2022 (top) and their cross-correlation as a function of lag (bottom). Positive lag indicates that air–sea heat flux leads SST. The maximum correlation occurs at ~2 months, consistent with delayed SST response due to mixed-layer heat storage.

Table S2. Comparison of MHW metrics obtained using a 20-year baseline (2003–2022) versus a 30-year baseline (1993–2022) using GLORYS12 near surface temperature. For each subregion (GAM and CS; Figure 1), we report the mean number of MHW days per year, mean MHW intensity (°C), and the standard deviation of intensity (°C). Diagnostics follow the Hobday et al. definition of MHWs.

	GAM 20	*GAM* 30	*CS* 20	*CS* 30
N° days of MHW per year	38.8	37.5	39.1	39.2
Mean intensity (°C)	0.77	0.78	0.76	0.78
Standard deviation (°C)	0.15	0.15	0.16	0.14

Table S3. Correlation coefficients between EOF principal components and climate indices, including effective degrees of freedom (DoF) and significance levels after low-pass filtering.

PC-index	*Filter*	*correlation*	*DoF*	*Significance*
PC1–MEI	2-yr	0.49	14	90%
PC1–WHWP	2-yr	0.58	14	95%
PC1–LHF	2-yr	0.73	14	99%
PC2–TNA	2-yr	0.53	14	90%
PC1–NAO	5-yr	0.90	6	95%

Reference

González-De Zayas, R., Pupo, F. M., González, J. A. L., and Hernández-Fernández, L.: Temporal behavior of air and sea surface temperature in a marine protected area of Cuba: the Jardines de la Reina National Park, Holos Environment, 22, 46–64, https://doi.org/10.14295/holos.v22i1.12472, 2022.